Available online at www.sciencedirect.com
ScienceDirect
International Journal of Thermal Sciences 46 (2007) 1232–1241
International Journal of Thermal Sciences
www.elsevier.com/locate/ijts

Turbulent natural convection in an enclosure with localized heating from below

Anil Kumar Sharma [a], K. Velusamy [a], C. Balaji [b,*]

[a] *Safety Engineering Division, Safety Group, Indira Gandhi Center for Atomic Research, Department of Atomic Energy, Kalpakkam 603102, India*
[b] *Heat Transfer and Thermal Power Laboratory, Department of Mechanical Engineering, Indian Institute of Technology Madras, Chennai 600 036, India*

Received 10 August 2006; received in revised form 27 October 2006; accepted 8 January 2007

Available online 28 February 2007

Abstract

This study reports the results of a numerical investigation of turbulent natural convection in a square enclosure with localized heating from below and symmetrical cooling from the vertical side walls. The present study simulates the case of an accidental heat generation due to fire in a typical isolated building of a nuclear reactor or electronic components cabin. The source of fire is considered to be centrally located at the bottom wall with different heated widths, which is assumed to be either isothermal or with isoflux. For the purpose of the analysis, the source length is varied from 20 to 80% of the total width of the bottom wall. The top wall and the unheated portion of the bottom wall are considered to be adiabatic, whereas sidewalls are isothermal. Steady as well as transient forms of two-dimensional Reynolds–Averaged-Navier–Stokes equations and conservation equations of mass and energy, coupled with the Boussinesq approximation, are solved by the control volume based discretisation method employing the SIMPLE algorithm for pressure–velocity coupling. Turbulence is modeled using the standard k–ε model. Rayleigh number, Ra, based on the enclosure height is varied from 10^8 to 10^{12}. Stream lines and isotherms are presented for various combinations of Ra and the heated width. A double cell flow pattern is observed with marginal loss in symmetry as Ra increases. The results are reported in the form of local and average Nusselt number on the heated floor. Correlations are developed to predict the heat transfer rates from the enclosure as a function of dimensionless heated width of the bottom wall and Ra, by least square linear regression analysis.

Keywords: Turbulent natural convection; Standard k–ε turbulence model; Square enclosure; SIMPLE algorithm

1. Introduction

Nuclear power plants have many interconnected buildings similar to other power plants. These buildings house equipment and instruments which are essential for the safe operation of the plant. They invariably contain significant quantities of combustible materials such as liquid sodium, electrical cables, fuel and lubrication oils and furniture. In the unlikely event of a fire in any such building or compartment, it is imperative that the fire is detected in time and necessary safety actions are taken to safeguard the adjacent buildings. Adequate design features need to be provided so that fire propagation to adjacent compartments is minimized. Moreover, knowledge of severity of such fire and the fire barrier rating necessary for the common walls of the compartments, is essential.

When liquid sodium or oil leaks from pipelines, it gets collected on the floor of the building at certain locations and burns at some specific rate depending upon the nature of the combustibles. The heat of combustion is transferred to the adjacent walls of the compartment, by natural convection and surface radiation in unventilated buildings. The same is absorbed by the walls depending upon their thermal capacity and finally transferred to the adjacent compartments. The size of the industrial compartments is generally large resulting in turbulent natural convection. The schematic diagram of a typical enclosure is depicted in Fig. 1. From this figure, it can be seen that, in the event of a leak in the sodium pipe line, the transfer of heat from the hot pool of liquid sodium to the medium in the enclosure (usually air like fluid) can be modeled as an enclosure with the bottom wall heated. The top wall can be considered to be adi-

* Corresponding author. Tel.: (+91 44) 22574689 (O); fax: (+91 44) 225770509.
E-mail address: balaji@iitm.ac.in (C. Balaji).

1290-0729/$ – see front matter © 2007 Elsevier Masson SAS. All rights reserved.
doi:10.1016/j.ijthermalsci.2007.01.010

Nomenclature

C_p	isobaric specific heat of the fluid	J/kg K
C_μ, $C_{\varepsilon 1}$, $C_{\varepsilon 2}$, $C_{\varepsilon 3}$	constants of the turbulence model	
g	acceleration due to gravity, 9.81	m/s^2
H	height of the enclosure	m
K	thermal conductivity of fluid	W/m K
k	turbulent kinetic energy	m^2/s^2
L	width of the heated portion on the bottom wall	m
Nu	Nusselt number	
Pr	Prandtl number, ν/α	
q''	heat flux	W/m^2
Ra	Rayleigh number, $g\beta\Delta T W^3/\nu\alpha$ or $g\beta W^4 q''/\nu\alpha K$	
T	temperature	K
t	time	s
Δt	time step	s
ΔT	temperature difference between the hot and cold walls	K
u, v	horizontal and vertical velocity components	m/s
u_t	friction velocity $\sqrt{\tau_w/\rho}$	m/s
W	width of the enclosure	m
x, y	horizontal and vertical coordinates	m
y^+	dimensionless wall distance, $y_n u_t/\nu$	
y_n	normal distance of the cell centre from nearest wall	m

Greek symbols

α	thermal diffusivity of fluid	m^2/s
β	isobaric cubical expansion coefficient of fluid	K^{-1}
λ	non-dimensional heated width, L/W	
ε	dissipation rate of turbulent kinetic energy	m^2/s^3
ψ	stream function	m^2/s
μ	dynamic viscosity of the fluid	Ns/m^2
μ_t	turbulent viscosity	Ns/m^2
ν	kinematic viscosity of fluid	m^2/s
ρ	density of the fluid	kg/m^3
σ_k, σ_T, σ_ε	turbulent Prandtl numbers of k, T and ε	
τ_w	wall shear stress	N/m^2

Subscripts

c	cold wall
eff	effective value
h	hot wall
max	maximum value
min	minimum value
t	turbulent

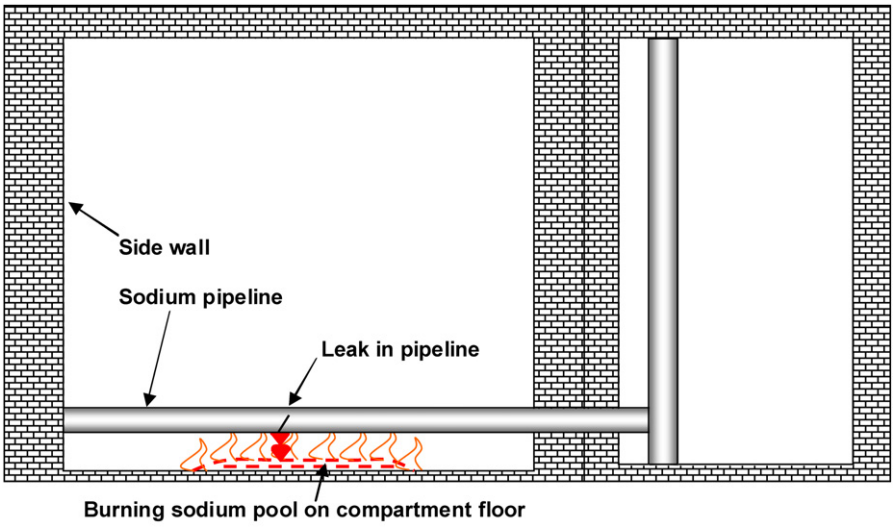

Fig. 1. Schematic of the practical enclosure.

abatic as it invariably houses a fire barrier. The side walls can be assumed to be cold and isothermal because of the following reasons (i) these are usually cooled and (ii) thermal inertia is so high that the heat release from the sodium pool can be absorbed by them, without significant change in their temperature. Considering the above reasons, the discussed problem can be simplified as a case of turbulent natural convection in an enclosure as indicated schematically, in Fig. 2.

The phenomenon of turbulent natural convection above horizontal heated surfaces has received considerable attention in the recent past. Applications of such analysis range from thermal design of buildings, location and design of safety alarms to thermal energy storage systems and electronic cabin cooling. Most of the studies dealing with turbulent natural convection in enclosures consider differentially heated vertical walls and adiabatic horizontal bottom walls. However, many practical applications, such as fire in a compartment, as discussed above, depart from this basic situation. In such applications, the heat source is at the bottom floor and the side walls are isothermal and cold. The temperature of the side walls can also be lower

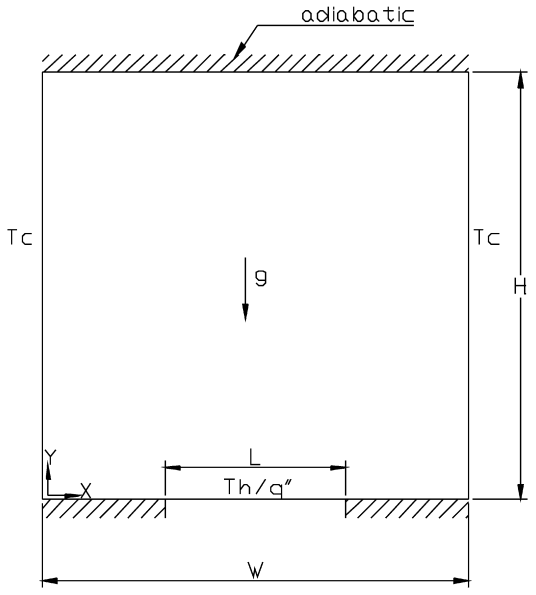

Fig. 2. Physical model and boundary conditions.

than ambient, depending on whether cooling strategies are used, as in the case of a reactor containment building. Natural convection heat transfer characteristics depend strongly on the location of the heat sources and heat sink. Hence, the practical situation discussed above needs special attention.

November and Nansteel [1] studied, analytically and numerically, steady natural convection in square enclosures heated from below and cooled along one side. The study indicated that the boundary condition of heating from below is quite different from the case of cooling from below and heating on one vertical wall. Asymptotic expressions were found for the temperature and heat transfer rates near the flux singularity on the enclosure floor. Hasnaoui et al. [2] numerically investigated laminar natural convection in an enclosure, with localized heating from below and cooled from the top at constant temperature, by a finite difference procedure. The key parameters of the problem were the cavity aspect ratio, position of the heat source and the Rayleigh number. The conclusion from the study indicated multiple steady state solutions for a given set of governing parameters.

Ganzarolli and Milanez [3] investigated natural convection in rectangular enclosures heated from below and symmetrically cooled from the sides using the stream function-vorticity formulation for Rayleigh numbers ranging from 10^3 to 10^7 and aspect ratio varying from 1 to 9. The influences of Rayleigh number (*Ra*), Prandtl number (*Pr*) and aspect ratio on the motion and on the energy transport were reported. Numerical values of the Nusselt number as a function of *Ra* were also reported with little influence of *Pr*. Anderson and Lauriat [4] studied flow in a square enclosure with a uniform flux and isothermal heating condition on the lower surface while one vertical wall was cooled isothermally. Experimental observations confirmed the absence of Benard-type instabilities for flux *Ra* numbers as large as 5×10^{13}. Aydin and Yang [5], numerically, studied laminar natural convection of air in a two-dimensional, rectangular enclosure with localized heating from below and symmetric cooling from the sides. Their analysis included the influence of the heated portion width and *Ra* on the fluid flow and heat transfer. They found the flow and temperature fields to be symmetric about the mid-width of the enclosure, due to symmetry of the boundary conditions. Sarris et al. [6] carried out a numerical study of natural convection in rectangular tanks heated locally from below. Based on numerical predictions, the effects of *Ra* and the geometry of the heated strip and the tank on the flow patterns and heat transfer were investigated for *Ra* in the range 10^2 to 10^7. Their study indicated that the augmentation of flow circulation intensity increases with an increase in the tank length and strip width. An experimental and numerical study of free convective heat transfer in square enclosures, heated from below was carried out by Calcagni et al. [7], for a Rayleigh number range of 10^3 to 10^6. The local Nusselt number on the heat source surface was given special attention. The variation of the local Nusselt number on the heat source and average Nusselt number were presented in their study. Holographic interferometry technique in real time and double exposure were used in the experimental method to obtain the visualization of possible oscillations of the plume and steady state temperature distribution inside the cavity respectively. Sharif and Mohammad [8] studied natural convection in rectangular cavities, using a finite volume based computational method. They considered a constant flux heating at the bottom and isothermal cooling from the sidewalls while the top wall was adiabatic. The length of the heat source was varied from 20 to 80 percent of W, for the range of Grashof number from 10^3 to 10^6. It was concluded that at lower Grashof number ($Gr \leqslant 10^4$), the heat transfer mechanism is dominated by diffusion whereas, for Grashof numbers greater than 10^5, buoyancy driven convection dominates. They found that the average Nusselt number and the maximum temperature are functions of aspect ratio and the length of the heat source. All of the above studies were carried out for the laminar regime.

The present study focuses on turbulent natural convection in an enclosure in which a part of the floor is heated at a constant temperature (first kind boundary condition) or by supplying with constant heat flux (second kind boundary condition). The study is performed in the range of *Ra* number 10^8 to 10^{12} with non-dimensional heated width ε varying from 0.2 to 0.8.

2. Mathematical formulation

2.1. Physical model and governing equations

Fig. 2 shows a schematic of the two-dimensional enclosure of width 'W', and height 'H', filled with air. The change in its density with temperature is incorporated through the Boussinesq approximation. The top wall and the unheated portion of the bottom wall are insulated, while the vertical side walls are isothermal at temperature, T_c and the bottom heated portion is either isothermal at a temperature T_h, or is subjected to a constant heat flux, q''.

The turbulent flow of air is described mathematically by the RANS equations, including the time averaged energy equation for the mean temperature field that drives the flow by the buoy-

ancy force. These equations in transient form along with the conservation equation for turbulent kinetic energy, k, and its dissipation rate ε are:

$$\frac{\partial \rho}{\partial t} + \frac{\partial}{\partial x}(\rho u) + \frac{\partial}{\partial y}(\rho v) = 0 \tag{1}$$

$$\frac{\partial(\rho u)}{\partial t} + \frac{\partial}{\partial x}(\rho uu) + \frac{\partial}{\partial y}(\rho vu) = -\frac{\partial p}{\partial x} + \frac{\partial}{\partial x}\left[2\mu_{\text{eff}}\frac{\partial u}{\partial x}\right] + \frac{\partial}{\partial y}\left[\mu_{\text{eff}}\left(\frac{\partial u}{\partial y} + \frac{\partial v}{\partial x}\right)\right] \tag{2}$$

$$\frac{\partial(\rho v)}{\partial t} + \frac{\partial}{\partial x}(\rho uv) + \frac{\partial}{\partial y}(\rho vv) = -\frac{\partial p}{\partial y} + \frac{\partial}{\partial x}\left[\mu_{\text{eff}}\left(\frac{\partial v}{\partial x} + \frac{\partial u}{\partial y}\right)\right] + \frac{\partial}{\partial y}\left[2\mu_{\text{eff}}\frac{\partial v}{\partial y}\right] + \rho\beta g(T - T_0) \tag{3}$$

$$\frac{\partial(\rho c_p T)}{\partial t} + \frac{\partial}{\partial x}(\rho u C_p T) + \frac{\partial}{\partial y}(\rho v C_p T) = \frac{\partial}{\partial x}\left[K_{\text{eff}}\frac{\partial T}{\partial x}\right] + \frac{\partial}{\partial y}\left[K_{\text{eff}}\frac{\partial T}{\partial y}\right] \tag{4}$$

$$\frac{\partial(\rho k)}{\partial t} + \frac{\partial}{\partial x}(\rho uk) + \frac{\partial}{\partial y}(\rho vk) = \frac{\partial}{\partial x}\left[\left(\mu + \frac{\mu_t}{\sigma_k}\right)\frac{\partial k}{\partial x}\right] + \frac{\partial}{\partial y}\left[\left(\mu + \frac{\mu_t}{\sigma_k}\right)\right]\frac{\partial k}{\partial y} + p_k + G_k - \rho\varepsilon \tag{5}$$

$$\frac{\partial(\rho\varepsilon)}{\partial t} + \frac{\partial}{\partial x}(\rho u\varepsilon) + \frac{\partial}{\partial y}(\rho v\varepsilon) = \frac{\partial}{\partial x}\left[\left(\mu + \frac{\mu_t}{\sigma_\varepsilon}\right)\frac{\partial \varepsilon}{\partial x}\right] + \frac{\partial}{\partial y}\left[\left(\mu + \frac{\mu_t}{\sigma_\varepsilon}\right)\right]\frac{\partial \varepsilon}{\partial y} + \left[C_{\varepsilon 1}(P_k + C_{\varepsilon 3}G_k) - C_{\varepsilon 2}\varepsilon\right]\frac{\varepsilon}{k} \tag{6}$$

where

$$P_k = \mu_t\left[2\left(\frac{\partial u}{\partial x}\right)^2 + 2\left(\frac{\partial v}{\partial y}\right)^2 + \left(\frac{\partial u}{\partial y} + \frac{\partial v}{\partial x}\right)^2\right]$$

$$G_k = -\frac{\mu_t}{\sigma_T}g\beta\frac{\partial T}{\partial y}; \qquad \mu_{\text{eff}} = \mu + \mu_t$$

$$\mu_t = C_\mu\frac{\rho k^2}{\varepsilon} \quad \text{and} \quad K_{\text{eff}} = K + \frac{\mu_t c_p}{\sigma_T}$$

For k–ε turbulence model, the constants used are

$$C_\mu = 0.09; \quad C_{\varepsilon 1} = 1.44; \quad C_{\varepsilon 2} = 1.92; \quad \sigma_T = 1.0$$

$$\sigma_K = 1.0 \quad \text{and} \quad \sigma_\varepsilon = 1.3$$

The value of, $C_{\varepsilon 3}$ is taken as $\tanh(v/u)$, as suggested by Henkes [9]. No wall functions are used and sufficiently fine grids are employed close to the walls to enable integration up to the walls.

2.2. Boundary conditions

The boundary conditions for the problem are specified as follows:

- Left and right walls:

  $u = v = k = 0, \quad T = T_c \quad \text{and} \quad \varepsilon = \infty$

- Bottom wall:

  $u = v = k = 0 \quad \text{and} \quad \varepsilon = \infty$

  $\dfrac{\partial T}{\partial y} = 0,$

  $\quad \text{for } 0 \leqslant x \leqslant \left(\dfrac{1-\lambda}{2}\right)W \text{ and } \left(\dfrac{1+\lambda}{2}\right)W \leqslant x \leqslant W$

  $T = T_h \quad \text{or} \quad -k\dfrac{\partial T}{\partial y} = q''$

  $\quad \text{for } \left(\dfrac{1-\lambda}{2}\right)W \leqslant x \leqslant \left(\dfrac{1+\lambda}{2}\right)W$

- Top wall:

  $\dfrac{\partial T}{\partial y} = 0, \quad u = v = k = 0 \quad \text{and} \quad \varepsilon = \infty$

2.3. Solution methodology

2.3.1. Steady state simulation methodology

For the numerical solution of these equations, the primitive variable (i.e. velocity and pressure) approach is adopted. The spatial derivatives in the equations are discretized using the finite-volume method. The enclosure is filled with a non-uniform rectangular staggered grid, whose minimum size near the walls is about 5×10^{-5} for accurately resolving the steep gradients in the thin buoyancy-driven boundary layers. A grid distribution scheme, suggested by Henkes [9], is used to enable fine grids near the walls and coarse grids away from the walls which results in very low values of y^+ (where, $y^+ = y_n u_\tau/\nu$, u_τ is the frictional velocity given by $\sqrt{\tau_w/\rho}$ and τ_w is the wall shear stress). These low values of y^+ (<0.35) imply that the present calculations can resolve even the viscous sub-layer. The SIMPLE algorithm proposed by Patankar and Spalding [10], is used to resolve the pressure–velocity coupling. The discretised equations are solved by the line by line Thomas algorithm, using two directional sweeps.

In order to determine the convergence of the iterative solutions, the absolute sum of the errors in the discretisation equations of all the control volumes for any variable Φ, $\sum_{i=1}^{N} |a_p\phi_p - \sum a_{nb}\phi_{nb} - b|_i$ is calculated and normalized with respect to a reference value, where N is the total number of control volumes, a_p is the coefficient of the discretisation equation corresponding to the control volume under consideration, a_{nb} are the coefficients of the discretisation equation corresponding to the neighboring control volumes and b is the source term [11]. Φ represents u, v, T, k or ε depending on the equation being equations. The reference value for normalization of error in the continuity equation is the circulation mass flow rate i.e. $\int_0^{w/2} \rho v_{y=H/2}\,dx$. For the momentum equations, it is the product of circulation mass flow rate and maximum velocity in the domain. For the energy equation, it is the product of circulation mass flow rate, specific heat and the temperature difference between the hot and cold walls. Similarly for the k

and ε equations, it is the product of mass flow rate and maximum values of k and ε inside the domain. Upon convergence, the normalized absolute sum of errors for any variable must be less than 10^{-3}. It may be mentioned that no significant change in the results is observed when this value is set to 10^{-4}. In addition to the errors, important parameters viz. Nusselt number, heat transfer rates for various walls and the variables u, v, T, k and ε at selected control volumes are monitored throughout the iterations. On convergence, the global imbalance in the heat transfer rates among the walls should be less than 0.1%.

For the case of first kind of boundary condition (i.e. constant temperature for the heated part), the average Nusselt number for the heated dimensionless length, λ, at the enclosure floor is calculated as

$$Nu = \frac{Q}{K(T_h - T_c)} \tag{7}$$

$$\text{with } Q = -\int_{\frac{1-\lambda}{2}}^{\frac{1+\lambda}{2}} K\left(\frac{\partial T}{\partial y}\right)_{y=0} dx \tag{8}$$

For the case of second kind of boundary condition, where uniform heat flux is specified at the enclosure floor, the local Nusselt number is calculated from

$$Nu_x = \frac{q'' W}{K[T_h(x) - T_c]} \tag{9}$$

Since the local Nusselt number is a function of x, the average Nusselt number is calculated as

$$Nu = \frac{\int_{\frac{1-\lambda}{2}}^{\frac{1+\lambda}{2}} Nu_x \, dx}{\int_{\frac{1-\lambda}{2}}^{\frac{1+\lambda}{2}} dx} \tag{10}$$

2.4. Transient simulation methodology

The geometry under consideration resembles a bottom heated cavity and in general, steady state solutions for such cases are viewed with skepticism. Hence, the time dependent forms of Eqs. (1)–(6) have also been solved to investigate the possibility of instability in the natural convection process, where the floor of the enclosure is heated. A fully implicit method has been used for the time integration. At any time step, the solution is considered to be converged when the normalized absolute sum of the residuals in the discretisation equations are reduced by at least three orders of magnitude. The time step, Δt, is chosen from time step independence studies. It is found that a time step of 0.01 s is optimum. Initial conditions used in the transient simulations are $u = v = 0$ and $T = T_c$.

3. Grid independence study and validation

To test the grid independence of the numerical scheme, solutions have been obtained on three non-uniform grid patterns viz. 46×42, 66×42 and 66×62. The average Nusselt number on the hot wall for a non-dimensional heated width of $\lambda = 0.8$ and $Ra = 10^{10}$, predicted by these mesh patterns are compared in Table 1. The difference in the average Nusselt number between the grid pattern of 66×42 (basic mesh) and that of 46×42 is 2.03%, while that between the 66×42 grid and 66×62 grid is only 0.07%. Hence, a grid pattern of 66×42 has been used in all the subsequent computations.

Table 1
Results of the grid independence study for $Ra = 10^{10}$ and $\lambda = 0.8$

Sl no.	Grid size	Average Nu	% Change
1	46×42	228.32	–
2	66×42	233.04	2.03
3	66×62	233.21	0.07

Table 2
Comparison of average Nusselt number (present study) with experimental and numerical studies of Calcagni et al. [7] and Aydin and Yang [5]

Rayleigh number	Average Nu		
	Present study	Calcagni et al. [7]	Aydin and Yang [5]
10^4	3.76	4.0	3.9
10^5	6.15	6.3	6.2
10^6	12.84	12.0	11.3

Table 3
Coefficients for the fitted polynomial curve of experimental temperature profiles at horizontal walls

Wall	a	b	c	d
Top	−259.23	253.08	−91.211	321.55
Bottom	−249.47	318	−147.48	320.3

For the purposes of validation, the results obtained from the present study are compared with the experimental and numerical results of Calcagni et al. [7] and Aydin and Yang [5] respectively with similar boundary conditions in the laminar regime. The average Nusselt numbers for a bottom heated square enclosure with non-dimensional heated width of 0.8 are compared in Table 2, along with the results obtained from the present simulations, in the laminar regime. It is clear that the agreement is good.

To validate the code for turbulent regime, a comparison is made with the experimental benchmark data of Ampofo and Karayiannis [12], for a side heated air filled vertical square cavity. The hot and cold walls of the cavity are isothermal at 323 and 283 K respectively, leading to a Rayleigh number of 1.58×10^9. As adiabatic conditions in the horizontal walls could not be maintained in the experiments, the measured temperature distribution of these walls is imposed in the present numerical simulations. A cubic polynomial, $ax^3 + bx^2 + cx + d$, is found to fit well with the measured data of horizontal wall temperature distribution with a correlation coefficient of 0.995 (see Fig. 3). The values of polynomial coefficients for the top and bottom walls are given in Table 3.

The distribution of local Nusselt number on the hot vertical wall is compared in Fig. 4(a) with the experimental data of [12]. A good agreement is observed between numerical and experimental data. Similarly, the predicted mid-height vertical velocity distribution adjacent to the hot wall is compared with

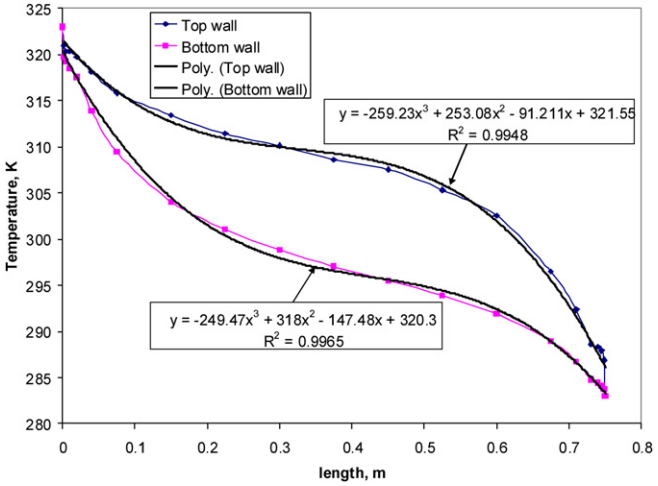

Fig. 3. Experimental mean temperature profiles on the horizontal walls.

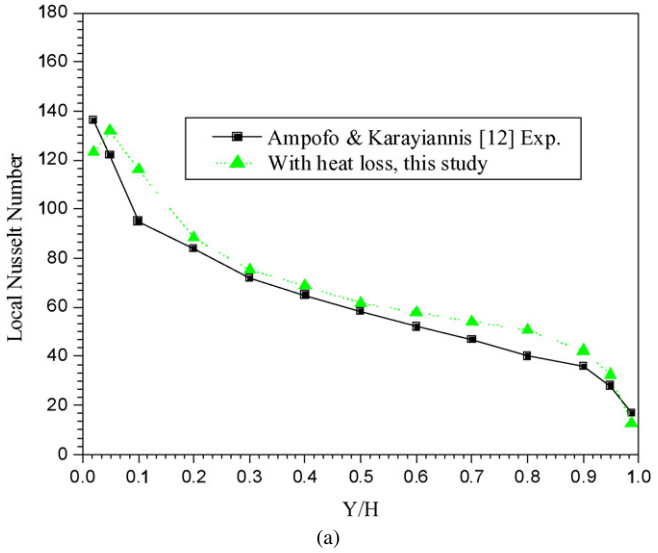

(a)

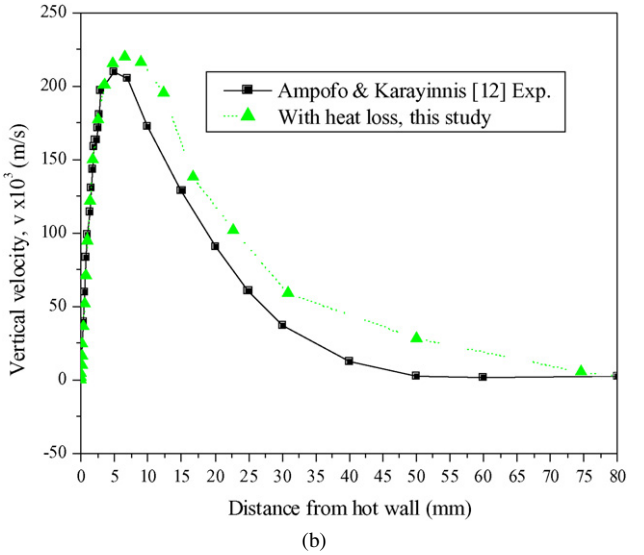

(b)

Fig. 4. Comparison of (a) hot wall Nusselt number distribution and (b) vertical velocity distribution at mid-height.

the measured data in Fig. 4(b). The comparison is again good, validating the computational model.

4. Sensitivity analysis of the near wall treatment

For natural convection flow and heat transfer, near wall resolution is of concern in numerical simulations. For example, recently Joubert et al. [13] carried out a numerical exercise for turbulent natural convection and pollutant diffusion in a two-dimensional partially partitioned cavity. The aim of this study was to compare the predictions of different turbulent models for natural convection at high Rayleigh numbers for applications such as energy saving, fire safety and thermal comfort. The study was carried out by using commercial CFD codes viz. FLUENT, PHOENICS, STAR-CD, N3S and in-house software. In this study, a two layer model was used for the near wall treatment in different codes. The main discrepancy between the results of various participants was observed to be the distribution of turbulent kinetic energy. The various simulations solving the RANS equations exhibited large values of k within the boundary layer, while LES and DNS predict very low values of k within the boundary layer. The study concluded that computed Nusselt numbers lie within $\pm 25\%$ range. The use of wall function was found to over predict the turbulent kinetic energy and Nusselt number, because a nonzero turbulent kinetic energy production is imposed at the first grid point when using wall functions.

In the present study, no wall functions are used and to resolve the thin viscous sub-layer within the boundary layer sufficiently fine grids are employed close to the walls to enable integration up to the walls. On the walls, turbulent kinetic energy is set to zero and its dissipation rate is set to infinity. For numerical implementation, ε is set to 10^{25} at the walls and the effect of this numerical value on the solutions is investigated in detail. The value of ε at the wall is varied from a very low value of 10

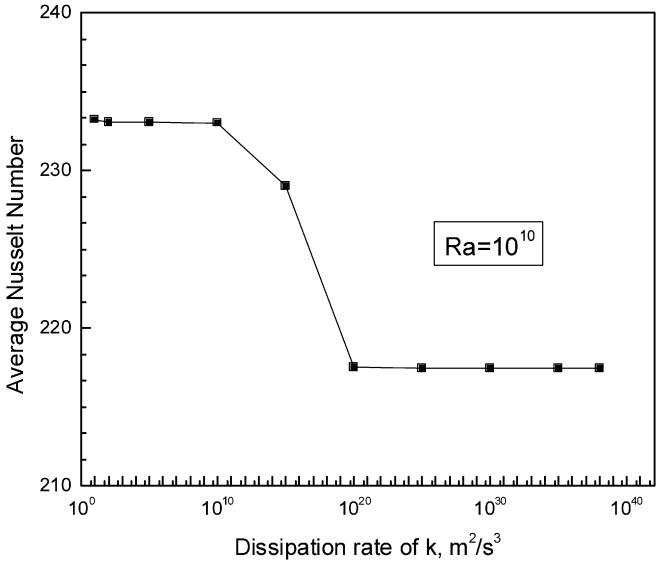

Fig. 5. Dependence of average Nusselt number on the value of ε at wall ($Ra = 10^{10}$).

to a very large value of 10^{38}. Fig. 5 shows the variation of the average Nusselt number with ε for a typical case of $Ra = 10^{10}$. It can be seen that the average Nusselt number remains constant for all the numerical values $\geqslant 10^{22}$, justifying the use of 10^{25} in the simulations.

The detailed validations serve to underscore the adequacy of the k–ε turbulence model for enclosures under conditions similar to the problem under consideration.

5. Results and discussion

Computations have been carried out for a total of 40 cases with the first and second kinds of boundary conditions at the bottom wall of the enclosure and five cases of transient simulations with isothermal heating at the bottom wall. The results cover a wide range of Rayleigh numbers (10^8–10^{12}). The working fluid is air with Prandtl number, $Pr = 0.71$. The non-dimensional heated width at the bottom wall, λ, is varied from 0.2–0.8. The predicted flow and temperature fields are shown in the forms of streamlines and isotherms, with 20 equally spaced contour levels.

The problem under investigation corresponds to a situation of unstable stratification with the bottom wall heated. Though the focus of the current study is only steady state solutions, it is essential to verify the adequacy of steady state solutions. Hence, results have been obtained by solving the transient form of the governing equations for Ra range of 10^8–10^{12} and for a fixed non-dimensional heated width of $\lambda = 0.8$. The evolution of average Nusselt numbers on the left, right and the bottom walls as a function of time are presented in Fig. 6. It can be seen that the Nusselt numbers reach non-oscillatory stable values of steady value after about 150 seconds. Also, these stable values of Nusselt numbers are exactly the same as those predicted by solving the steady state form of the governing equations, which are discussed in the subsequent sections. Thus, the results obtained from a transient solution of the equations demonstrate the adequacy of the steady state formulation for the present study.

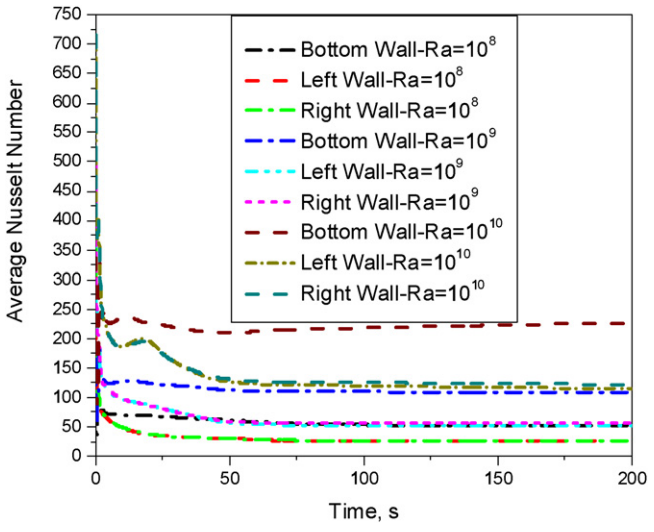

Fig. 6. Evolution of average wall Nusselt numbers for various values of Ra for $\lambda = 0.8$.

5.1. Flow and temperature fields with isothermal heating condition

Figs. 7(a)–(e) show the flow field and isotherms for $10^8 \leqslant Ra \leqslant 10^{12}$ with a non-dimensional heated width of 0.6. The plots are arranged in two columns, with the left column representing the stream functions and the right column representing the isotherms for increasing values of Ra. It is seen that two counter clockwise rotating cells are observed for all the values of Ra and λ. The fluid that is heated from the bottom rises along the mid-width and impinges at the top adiabatic wall, where it bifurcates and flows towards the vertical isothermal walls, replacing the cold fluid adjacent to them. Thus, two cells are formed both of which are of nearly equal strength. As Ra increases, the strength of the vortex also increases (see Fig. 7), with marginal distortion in the symmetry at high Rayleigh numbers. The isotherms display that the two opposing wall jets over the bottom wall travel towards each other, meet near the mid-width and form a plume. In the case of natural convection in enclosures, it is known that the velocity scales as $\sqrt{W}$. The maximum stream function which is the product of velocity and the enclosure width scales as $W^{3/2}$. Since Ra is proportional to W^3, the maximum stream function scales as $Ra^{1/2}$. The maximum stream function value depicted in Fig. 7 compares well with this scaling. For the case of $\lambda = 0.6$, the stream function value increases from 0.00587 to 0.346 when Ra number increases from 10^8 to 10^{12}. Figs. 8(a)–(c) depict the streamlines and isotherms in the enclosure for $Ra = 10^{12}$ for various values of the non-dimensional heated width. It is clear from these figures that the stream function values $\psi_{\min}$ and $\psi_{\max}$ are -0.308 and 0.308 respectively for the heated width $\lambda = 0.4$ and these are -0.379 and 0.385 respectively for $\lambda = 0.8$. This increase in the stream function value with λ is found to be almost linear for the entire range of Ra considered in the present study, as shown in Fig. 9. This figure indicates the variation of $\psi_{\max}$ with λ for $Ra = 10^{12}$. Thus, the intensity of the buoyancy induced flow increases linearly with the non-dimensional heated width. On comparing the isotherms in Fig. 7 for various values of Ra, it is observed that as Ra increases, the isotherms are packed near the bottom heated wall i.e. for large value of Ra, the temperature gradients are more severe near the heated bottom wall. This implies an increase in heat transfer from the enclosure for higher Ra. Similarly, as λ increases the heat transfer rate from the enclosure also increases.

The variation of the average Nusselt number with the heat source width, for various values of Ra is depicted in Fig. 10. It is clear that at low Ra, the Nusselt number is a weak function of λ. However, as Ra increases, the Nusselt number becomes a strong function of λ.

The Nusselt number is found to be minimal at almost the mid-point on the heated bottom wall. In view of the stagnation point being located at the mid-point, the convective heat transfer is the lowest at this point. The variation of the average Nusselt number at the bottom heated wall in the enclosure with Ra, for various values of the non-dimensional heated width, λ, is presented in Fig. 11 and the functional relationship between Nu and Ra turns out to be $Nu \sim Ra^{0.334}$ for the whole range of λ.

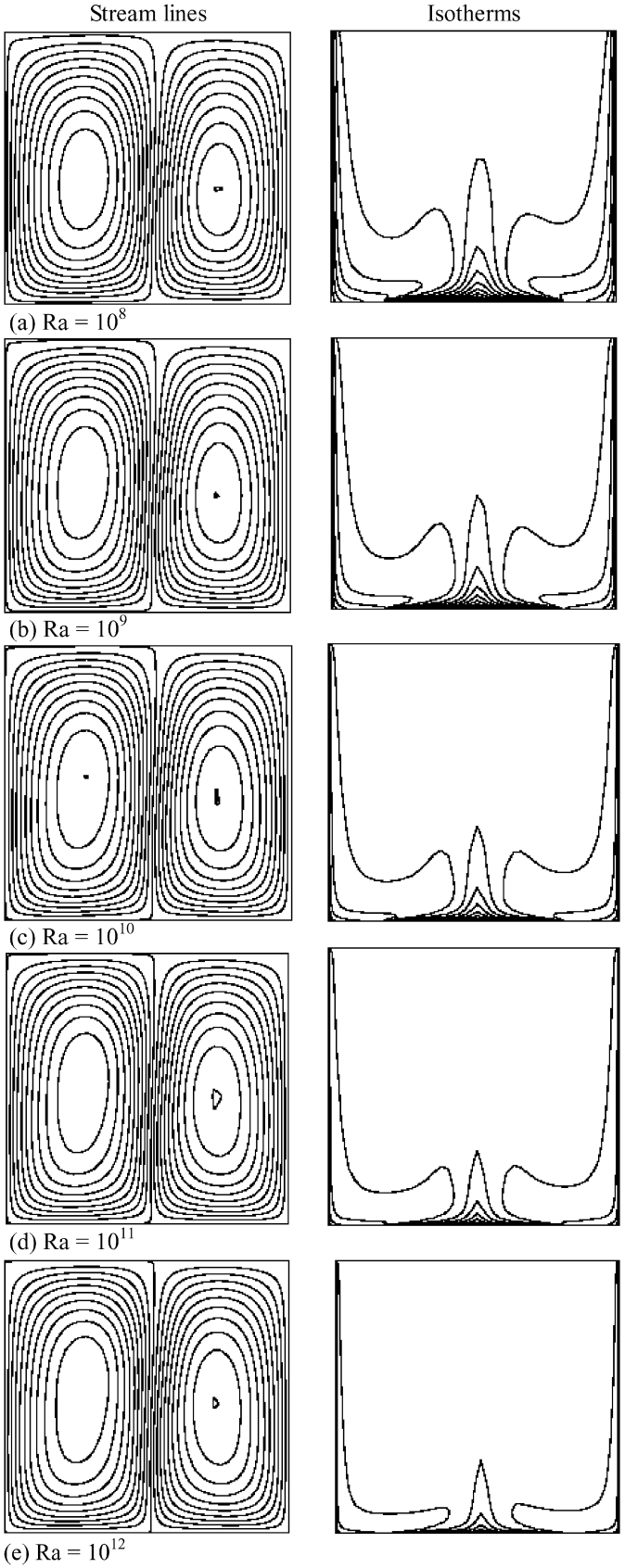

Fig. 7. Streamlines and isotherms for (a) $Ra = 10^8$, $\psi_{max} = 0.00587$, (b) $Ra = 10^9$, $\psi_{max} = 0.016$, (c) $Ra = 10^{10}$, $\psi_{max} = 0.044$, (d) $Ra = 10^{11}$, $\psi_{max} = 0.123$, (e) $Ra = 10^{12}$, $\psi_{max} = 0.346$, with non-dimensional heated width, $\lambda = 0.6$.

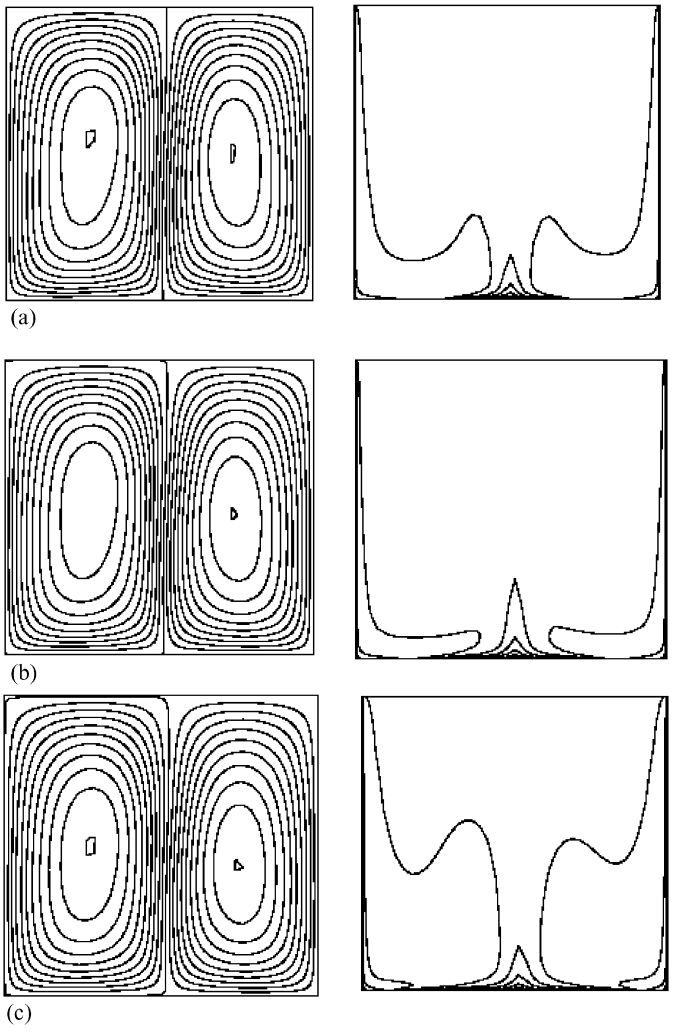

Fig. 8. Streamlines and isotherms in the enclosure for $Ra = 10^{12}$ with different heated width (a) $\lambda = 0.4$, $\psi_{max} = 0.308$, (b) $\lambda = 0.6$, $\psi_{max} = 0.346$ and (c) $\lambda = 0.8$, $\psi_{max} = 0.385$.

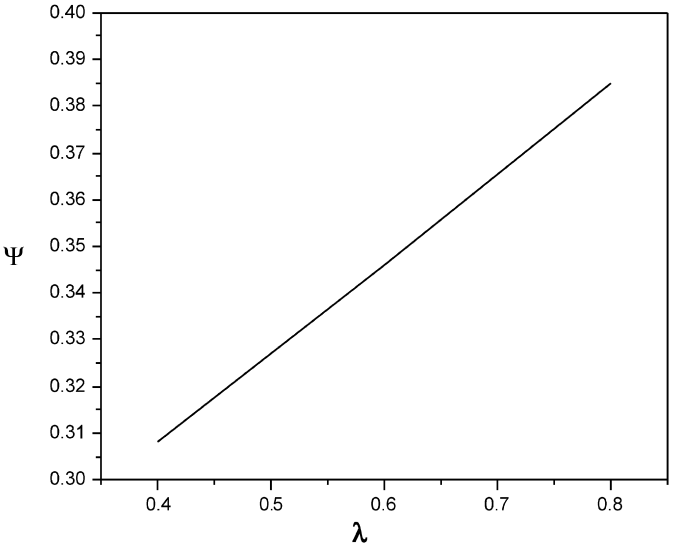

Fig. 9. Variation of the maximum stream function value, ψ_{max} with the non-dimensional heated width, λ for $Ra = 10^{12}$.

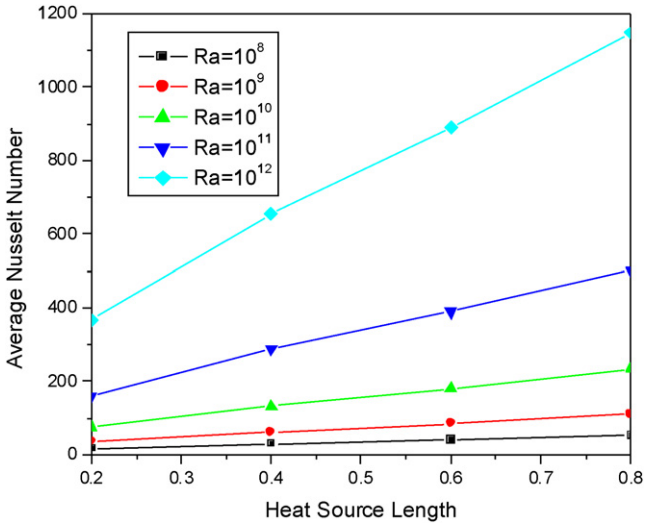

Fig. 10. Variation of average Nusselt number at heated wall with *Ra* for various values of λ (isothermal condition).

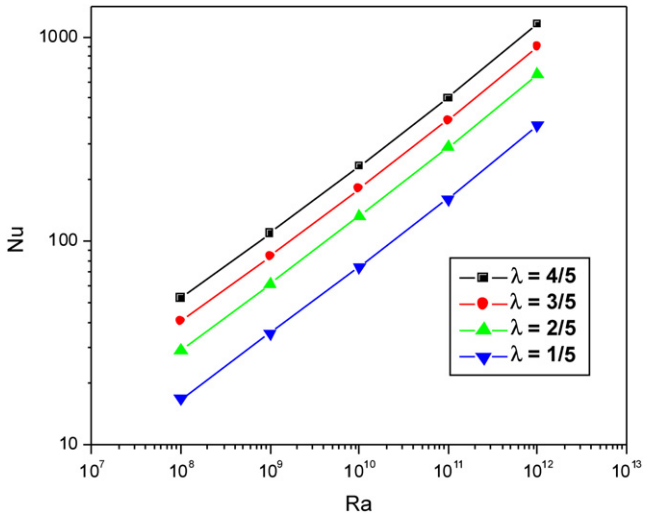

Fig. 11. Average Nusselt number versus Rayleigh number for different λ values.

A correlation is developed using least squares regression for the isothermal heating condition, to predict the heat transfer from the bottom wall of the enclosure, in terms of the non-dimensional heated width and *Ra*.

$$Nu = 0.13\lambda^{0.8} Ra^{0.334} \tag{11}$$

The correlation coefficient of the above equation is 99% and the data agree to within ±3% of those predicted by the above correlation for $10^8 \leqslant Ra \leqslant 10^{12}$ and $0.2 \leqslant \lambda \leqslant 0.8$.

5.2. *Flow and temperature fields with second kind of boundary condition*

The flow and temperature characteristics in the enclosure for the case of a specified heat flux at the bottom wall are given in this section. Figs. 12(a)–(b) show the stream function and isotherms for $Ra = 10^{10}$ and 10^{12} for a non-dimensional heated width of $\lambda = 0.6$. It is clearly seen from these figures that the flow consists of two counter clockwise rotating cells as

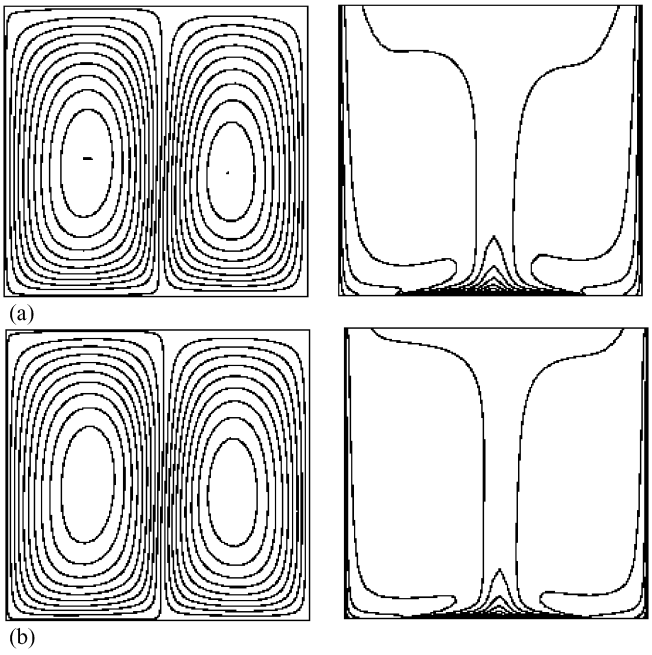

Fig. 12. Streamlines and isotherms for (a) $Ra = 10^{10}$, $\psi_{max} = 0.0067$, (b) $Ra = 10^{12}$, $\psi_{max} = 0.031$, with non-dimensional heated width, $\lambda = 0.6$.

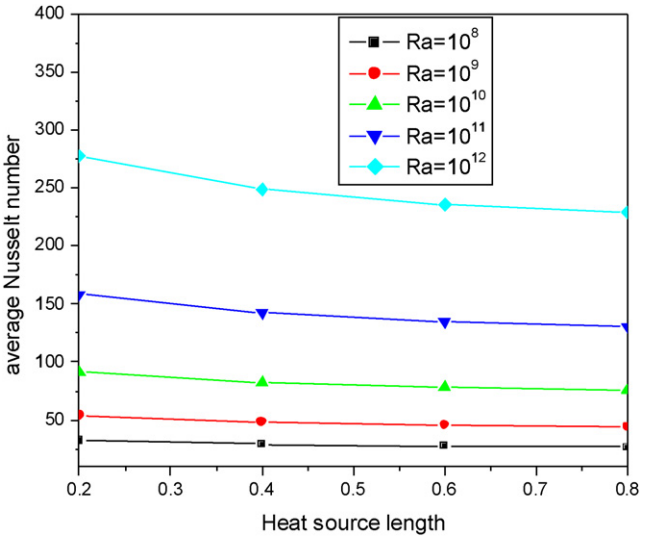

Fig. 13. Variation of average Nusselt number on the heated wall with *Ra* for various values of λ (isoflux condition).

in the case of the isothermal boundary condition but with reduced flow velocities. The flow intensity reduces by one order in this case compared to that observed for the isothermal case. For example, the maximum stream function value, ψ_{max}, for $Ra = 10^{12}$ is 0.031 for the isoflux condition, while the same for isothermal condition is 0.346 (see Figs. 7 and 12). For identical *Ra*, the isotherms indicate lower temperature levels in the enclosure with temperature stratification in the core region compared to that of isothermal heating. This is the reason for the reduced circulation inside the enclosure.

Fig. 13 shows the variation of average Nusselt number as a function of the heated width for $10^8 \leqslant Ra \leqslant 10^{12}$. It is clear that as the heat source width increases, *Nu* decreases. This is ex-

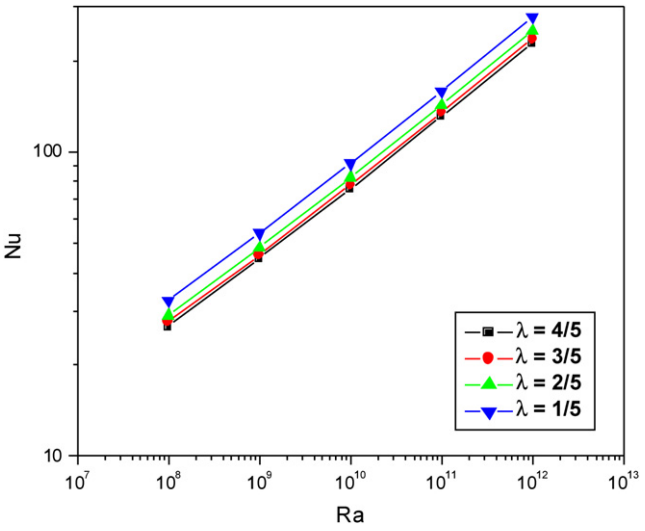

Fig. 14. Nusselt number as a function of Rayleigh number for different λ values (isoflux condition).

pected because as the source width increases, the temperature level of the bottom wall increases, leading to a reduction in the heat transfer coefficient, which is inversely proportional to the wall temperature, as can be seen from Eq. (9). Similar trends in the results have been seen by Sharif and Mohammad [8] for the laminar regime. This decrease in *Nu* is found to be marginal at lower values of *Ra*, compared to that at higher values of *Ra*. This trend is completely different from that observed in the case of isothermal heating, where *Nu* increases with increase in heated width.

Fig. 14 shows the values of average Nusselt number as a function of *Ra* for various heated widths. It is evident that the average Nusselt number varies as $Nu \sim Ra^{0.233}$. It is also clear that the *Nu* number in the case of isoflux heating is a weaker function of heated width when compared to the isothermal case.

Based on a parametric study, a correlation for the heat transfer rate has been proposed using multiple linear regression for the isoflux case, for $10^8 \leqslant Ra \leqslant 10^{12}$ and $0.2 \leqslant \lambda \leqslant 0.8$ as

$$Nu = 0.35\lambda^{-0.14} Ra^{0.233} \tag{12}$$

The above equation has a correlation coefficient of about 99% and the data agree to be within ±3% of the predicted Nusselt numbers.

6. Conclusions

Buoyancy induced turbulent flow and heat transfer of air inside a two-dimensional enclosure with localised heating at the bottom wall and isothermally cooled side walls was numerically investigated. The key parameters of interest are *Ra* and the dimensionless heat source length, for both isothermal and constant heat flux boundary conditions. Two counter clockwise rotating cells are observed for the entire range of *Ra* and non-dimensional heated width. The dependence of the Nusselt number on the heated width is found to be completely different for the isothermal and isoflux heating cases. In the case of isothermal heating, the Nusselt number increases with an increase in the heated width, while the opposite is true for the isoflux heating. It is also observed that the Nusselt number is a weak function of heated width for isoflux heating compared to that of isothermal heating. In the case of isoflux heating, the intensity of buoyancy induced flow is lower compared to that of isothermal heating for identical values of *Ra*. The flow intensity is found to increase linearly with the heated width in both the cases. For engineering applications, correlations have been developed by least square linear regression analysis to evaluate the Nusselt number in terms of the heated width and *Ra*, for both types of heating. The functional relationship between the Nusselt and Rayleigh numbers is $Nu \sim Ra^{0.334}$ for isothermal heating and $Nu \sim Ra^{0.233}$ for isoflux heating.

References

[1] M. November, M.W. Nansteel, Natural convection in rectangular enclosures heated from below and cooled along one side, Int. J. Heat Mass Transfer 30 (1987) 2433–2440.
[2] M. Hasnaoui, E. Bilgen, P. Vasseour, Natural convection heat transfer in rectangular cavities partially heated from below, J. Thermophys. Heat Transfer 6 (1992) 255–264.
[3] M.M. Ganzarolli, L.F. Milanez, Natural convection in rectangular enclosures heated from below and symmetrically cooled from the sides, Int. J. Heat Mass Transfer 38 (1995) 1063–1073.
[4] R. Anderson, G. Lauriat, The horizontal natural convection boundary layer regime in a closed cavity, in: Proceeding of 8th Int. Heat Transfer Conference, San Francisco, CA, 1986, pp. 1453–1458.
[5] O. Aydin, Wen-Jei-Yang, Natural convection in enclosures with localized heating from below and symmetrical cooling from sides, Int. J. Numer. Methods Heat Fluid Flow 10 (5) (2000) 518–529.
[6] I.E. Sarris, I. Lekakis, N.S. Vlachos, Natural convection in rectangular tanks heated locally from below, Int. J. Heat Mass Transfer 47 (2004) 3549–3563.
[7] B. Calcagni, F. Marsili, M. Paroncini, Natural convective heat transfer in square enclosures heated from below, Appl. Thermal Engrg. 25 (2005) 2522–2531.
[8] M.A.R. Sharif, T.R. Mohammad, Natural convection in cavities with constant flux heating at the bottom wall and isothermal cooling from the sidewalls, Int. J. Thermal Sci. 44 (2005) 865–878.
[9] R.A.W.M. Henkes, Natural convection boundary layers, PhD thesis, Delft University of Technology, The Netherlands, 1990.
[10] S.V. Patankar, D.B. Spalding, A calculation procedure for heat, mass and momentum transfer in three dimensional parabolic flows, Int. J. Heat Mass Transfer 15 (1972) 1787–1806.
[11] S.V. Patankar, Numerical Heat Transfer and Fluid Flow, Hemisphere, Washington, DC, 1980.
[12] F. Ampofo, T.G. Karayiannis, Experimental bench mark data for turbulent natural convection in an air filled square cavity, Int. J. Heat Mass Transfer 46 (2003) 3551–3572.
[13] P. Joubert, P.L. Quere, C. Beghein, B. Collignan, C. Stephane, G. Stephane, G. Dominique, L. Pierre, M. Marjorie, A. Sergent, V. Stephane, A numerical exercise for turbulent natural convection and pollutant diffusion in a two-dimensional partially portioned cavity, Int. J. Thermal Sci. 44 (2005) 311–322.